Supplementary materials for ”GPS constraints on deformation in northern Central America from 1999 to 2017, Part 2: Block rotations and fault slip rates, fault locking, and distributed deformation”

by A. Ellis *et al*.

Summary

The supplemental materials include figures that are referenced in the main document, explanatory text for some of the supplemental figures, and four tables in text format that list all the data we used for our TDEFNODE analysis, as follows:

1. Supplemental Figures 1 through 13, which are referenced in the main document.
2. The text table GPSVels_ITRF08.txt lists the GPS site velocities that were used for our analysis.
3. The text table CA_GPSVels_ITRF08.txt lists the Caribbean GPS site velocities that were used for our analysis.
4. The text table NA_GPSVels_ITRF08.txt lists the North America GPS site velocities that were used for our analysis.
5. The text table Flt_Eqs.txt lists the fault and earthquake slip directions that were used for our analysis.

1 GPS velocity field description and figures

The GPS velocity field in southern Mexico and northern Central America samples deformation from four major deforming zones, namely, the Motagua/Polochic fault zone, the Central America volcanic arc, the Middle America and southern Mexico subduction zones, and a triangular zone of distributed extension between the Motagua fault and Central America volcanic arc. The regional velocity field (Supplemental Figure 2) clearly shows the dextral shear and velocity gradient associated with the Motagua and Polochic faults, which cross-cut the entire GPS network. The deformation associated with the other features is more difficult to see when viewed at a regional scale, including the velocity gradients that are diagnostic of active, locked faults. This supplemental document thus includes multiple graphics that are designed to emphasize the cross-fault velocity gradients and changes in those gradients with distance along their associated fault zones. Below, we display and discuss these gradients for four tectonically distinct, but overlapping regions that encompass our study area.

1.1 Chiapas Tectonic Province

The only published velocity field for the Chiapas Tectonic Province and more generally, the broad deforming region north of the Polochic fault, included eight campaign sites and one continuous station from the Chiapas Tectonic Province, with data spanning up to four years (Franco *et al*. 2012). For the same area, our new velocity field includes eight continuous stations and seven campaign sites. Notably, the data from this region now span 14 years and include new campaign data from our reoccupations in 2015 of all but one of the campaign sites first reported by Franco *et al*. (2012).

Relative to the North America plate interior, all of the stations north of the Polochic fault move directly northeastward (Supplemental Figures 2 and 4 and Figure 9 in the main document) at rates that generally diminish inland. As a test, we used a simple forward elastic half-space model to predict the expected elastic response in our study region assuming that the Cocos-North America plate convergence velocities across the offshore subduction interface are given by the MORVEL angular velocity for this plate pair (DeMets *et al*. 2010) and that the offshore subduction interface is locked to a depth of 40 km, consistent with seismic and geodetic observations (White *et al*. 2004; Ye *et al*. 2013; Ellis *et al*. 2015). For this simple model, the trench-normal components of the measured station velocities (red circles in Supplemental Figure 4b) mostly fall between the 50 and 100 percent locking curves that are shown in the figure. This agrees with the moderate-to-strong locking that was previously estimated by Franco *et al*. (2012).

Descriptions and discussions of our inverse modeling results for this region are found in Sections 4.3 and 4.4 of the main document.

1.2 Motagua-Polochic fault zone velocity field and transects

Figure 11 from the main document displays the velocities of sites within ≈150 km of the Motagua-Polochic fault zone relative to a stationary Caribbean plate. Based on previous evidence that the slip rate across these faults diminishes to the west (Lyon-Caen *et al*. 2006; Franco *et al*.) 2012), we subdivided the numerous GPS sites within several hundred km of the fault zone into four distinct transects that collectively span the entire fault zone. In Supplemental Figures 5 and 6, we project the site velocities onto azimuths parallel to the primary fault segment within each transect. Short descriptions of the four transects follow.

For the easternmost and central transects (Supplemental Fig. 5), the velocities of the sites at the ends of the two transects differ by 17-18 mm yr^{-1} and define sharp S-shaped gradients that are centered on the Motagua fault. To first order, the velocities are well matched by a simple 1-D forward elastic half-space model of a strike-slip fault with a 17-19 mm yr^{-1} slip rate deficit and 15-km assumed locking depth (shown by the light gray lines in the figure). Interestingly, the velocity gradient that is defined by the velocities of the sites within 10 km of the Motagua fault is steeper than is predicted by our simple forward model, possibly indicating that the fault locking depth is shallower than the 15 km assumed for our simple model or that shallow creep accommodates some of the fault slip. Slip along the Motagua fault has juxtaposed serpentine rocks on both sides of the Motagua fault (Harlow *et al*. 2004; Brocard *et al*. 2016), which may promote aseismic creep (Reinen *et al*. 1991). Although our data are insufficient to make a compelling case for creep, the high seismic hazard of the fault warrants further investigation of this possibility.

Supplemental Figure 6 shows the velocity transects for the western portion of the fault zone, one that crosses both faults near the longitude of Guatemala City (Supplemental Figure 6a) and the other that crosses the western ≈100 km of the Polochic fault, but not the Motagua Fault (Supplemental Figure 6b. Both transects have exhibit smaller maximum velocity changes and more gradual velocity gradients than are observed for the eastern and central transects shown in Supplemental Figure 5. This agrees with the westward fault slip-rate decrease reported by Lyon-Caen *et al*. (2006). Descriptions of the modeling and interpretation of these site velocities is found in Section 4.6 of the main document.

1.3 Central America forearc sliver

Figures 7 and 8 show the components of GPS site velocities parallel to the Central America volcanic arc for sites within six arc-normal transects of the ≈900-km-long forearc sliver boundary in our study area. The velocities for sites in Nicaragua define a sigmoidal curve with a velocity step of 11 mm yr^{-1} (Figure 7a). Given that forearc sliver motion in much of Nicaragua appears to be accommodated by bookshelf faulting (LaFemina *et al.* 2002; Funk *et al.* 2009), the sigmoidal velocity pattern is not interpretable in the context of a simple locked, arc-parallel strike-slip fault. Bookshelf faulting and normal faulting within the Gulf of Fonseca and adjacent areas (Alvarado *et al.* 2011) similarly preclude a simple interpretation of the velocity pattern for the sites within the transect of the Gulf of Fonseca (Figure 7b). Results from modeling these velocities are described in Section 4.7.2 and 4.7.3 of the main document.

The central El Salvador transect (Figure 7c) crosses the Berlin, Lempa, and San Vicente strike-slip fault segments (located in Fig. 10b of the main document), which are the only locations along the volcanic arc where the movement of the forearc may be accommodated by a single structure. The ≈10-11 mm yr^{-1} difference between the velocities of the most distal sites in the transect is consistent with previous observations (Correa-Mora *et al.* 2009; Alvarado *et al.* 2011; Staller *et al.* 2016). The sigmoidal pattern that is defined by the velocities of the sites in this transect is evidence that the Berlin, Lempa, and San Vicente fault segments are locked, consistent with their long histories of destructive strike-slip earthquakes (White 1991; White & Harlow 1993). Simplistic 1-D elastic forward modeling variously assuming 5-km, 10-km, and 15-km locking depths for these faults suggests that they may be locked to a depth of only 5 km (solid gray curve in Figure 7c).

In western El Salvador, the forearc sliver movement is accommodated by a series of poorly understood, interconnected normal, bookshelf, and strike-slip faults that transfer the dextral slip several tens of kms inland between the western end of the San Vicente strike-slip fault and eastern end of the Jalpatagua fault in southeast Guatemala. The velocities of the most distal sites within this transect differ by ≈11-12 mm yr^{-1} (Figure 8a), similar to the velocity differences for the transects farther east (Figure 7).

The transects of the Jalpatagua fault (Figure 8b) and the volcanic arc west of the Guatemala City graben (Figure 8c) both have smaller end-to-end velocity changes than for the transects of El Salvador and Nicaragua. The Jalpatagua fault transect, which is populated mostly by campaign sites with short time series and high uncertainties (open circles in Figure 8b), suggests an upper slip rate limit of ≈8 mm yr^{-1}, several mm yr^{-1} slower than the Salvadoran transects. The velocities for sites in the westernmost transect, where nothing is known about the faults that may accommodate shear across the volcanic arc, change by only 0-2 mm yr^{-1} (Figure 8c). In Section 4.7.5 of the main document, we quantify the amount of slip that is transferred northward off from the volcanic arc faults into the Guatemala City graben and onto other normal faults north of the volcanic arc.

Modeling results and fits for all the GPS site velocities from the forearc and its boundaries are described and displayed in Section 4.7 of the main document.

2 Alternative models: Assumptions and inversion results

In order to evaluate the robustness of the preferred-model results that are described in the main document, we derived five alternative models by varying the modeling assumptions and/or constraints, the data, and the fault geometry that were used to derive the model. Below, we briefly describe how each alternative model differs from the preferred model described in the main document

2.1 Addition of a deforming Chiapas block

Given compelling seismic and structural evidence for distributed deformation of the North America plate in the southern Mexican state of Chiapas, we evaluated whether adding a distinct Chiapas block to our model significantly altered any of the block angular velocities or fault locking solutions relative to those for our preferred model. Supplemental Figures 11b and 13a show a subset of results for one realization of a TDEFNODE model with a deforming Chiapas block. None of the principal results differ significantly from those of our preferred model, nor does the fit change significantly.

2.2 Alternative geometry for the Middle America subduction interface

We evaluated the influence of modest changes in the Slab1.0 subduction interface geometry that is implicit in our preferred model by altering the Slab1.0 depth contours to create a shallower-sloping interface at depths above 15 km and more sharply curving interface between 15 km and 30 km to define an alternative interface geometry that is consistent with depth cross-sections we constructed from relocated Middle America subduction zone earthquakes. The results from an inversion with this modified geometry do not differ significantly from our other results (Panel E in Supplemental Figure 11).

2.3 Deep locking model: Middle America subduction interface

As part of our evaluation of the model robustness, we re-inverted all the data while allowing locking on the subduction interface to extend downward to a depth of 60 km, deeper than the 40-km maximum depth for our preferred solution. The primary effect of this change was an apparent downdip shift in the region of strong subduction locking off the coast of southern Mexico (Supplemental Figure 11f) versus models with shallower enforced locking depths (*e.g.* Supplemental Figures 11a-e). The suggested deep locking of the subduction interface in this region disagrees with the locations of subduction thrust earthquakes offshore, which are nearly all shallower than a 40-km depth (Supplemental Figure 3).

The fault slip rates estimated with this alternative model (Supplemental Figure 13b) all fall within the 95 percent uncertainties of the slip rates estimated with our preferred model.

2.4 Minimum- and maximum-locking subduction zone models

Based on important tradeoffs we observed between the degree of the subduction zone locking and the movement of the Central America forearc sliver, we tailored two approaches for estimating upper and lower bounds for the magnitude of locking along the Middle America subduction zone offshore from our study area. We estimated an upper bound by omitting from our inversion both of the *a priori* slip direction constraints that are imposed along the Nicaraguan volcanic arc in our preferred inversion, which we found (by trial and error) yields models with the highest degree of subduction locking offshore Nicaragua and El Salvador.

In order to estimate a lower bound for the subduction zone locking, which we refer to hereafter as a "minimum-locking model", we note that GPS sites from much of the Central American forearc move nearly parallel to the trench (Supplemental Figure 9), as might be expected for an unlocked subduction interface above which the forearc sliver translates freely. If this is true, then the directions of GPS sites on the forearc sliver can, in principle, be used to impose *a priori* constraints in an inversion in order to ensure that the forearc sliver moves largely parallel to the trench.

To accomplish the above, we inverted the directions of 33 GPS sites in the forearcs of western Nicaragua, El Salvador, and parts of southern Guatemala (shown by the red arrows in Supplemental Figure 9) to find the pole that best describes the rotation of the forearc relative to the Caribbean plate. Their best-fitting pole, which is located at 7.3°N, 91.4°W, has a WRMS misfit of $\approx$11°, equivalent to a $\approx$2 mm yr^{-1} WRMS misfit given the 10-12 mm yr^{-1} rates for most of these sites. From the dominantly trench-parallel directions of 7 GPS sites on the Fonseca block (purple arrows in Supplemental Fig. 9), we similarly determined a best-fitting pole of 2.9°N, 92.8°W, for which the WRMS misfit is only $\approx$2°.

We then used the best-fitting poles for the Central America forearc sliver and Fonseca block as *a priori* constraints in an inversion of the data that are described in Section 2 of the main document to derive the minimum-locking TDEFNODE model. Similar to our preferred model, the minimum locking model is constrained by the Cocos, Caribbean, and North America plate angular velocity constraints from Table 1 of the main document. The parameters estimated for the minimum-locking model include angular velocities for the Chortis, Ipala, and Motagua-Polochic blocks, angular rates for the forearc sliver and Fonseca block, and locking ratios and depths for the Middle America subduction interface and onshore strike-slip faults.

Supplemental Figure 11 compares the subduction zone locking solutions for our preferred (Panel A) to those for the minimum-locking and strong-locking models (Panels C and D in Supplemental Figure 11, respectively). Omitting the two *a priori* dextral-slip constraints along the Nicaraguan volcanic arc increases the average subduction interface locking to 27 percent versus 16 percent for our preferred solution.

In contrast, the average subduction zone locking is only 3 percent below the forearc sliver for the minimum-locking model, smaller than the 27 percent upper locking limit. Relative to our preferred model misfit, reduced chi-square for the minimum-locking model is $\approx$70 percent larger. Imposing the constraints that give rise to the minimum-locking solution thus significant degrades the fit to our GPS velocities.

2.5 Earthquake slip directions, GPS site velocities, and Cocos-forearc sliver motion

As a further check on the robustness of our Cocos-forearc sliver angular velocity and the consistency of the 201 GPS site velocities and 175 Middle America trench earthquake slip directions that are used in the preferred model to constrain the motion of the forearc sliver, we excluded all 175 slip directions from the Middle America trench thrust earthquakes and inverted the 201 GPS and remaining data and *a priori* constraints to estimate an alternative angular velocity for the Cocos-forearc sliver plate pair. The WRMS misfit to the 201 GPS site velocities for this alternative inversion, 1.03 mm yr^{-1}, differs insignificantly from the 1.00 mm yr^{-1} WRMS misfit for our preferred model and the convergence rates and directions predicted by the alternative Cocos-forearc sliver angular velocity differ by no more than 2.0 mm yr^{-1} and 0.1° from the preferred model estimates. We conclude that the 201 GPS site velocities and 175 Middle America trench earthquake slip directions provide mutually consistent kinematic information with regard to Cocos plate motion.

References in addition to those provided in the main document

Brocard, G., Anselmetti, F. S., & Teyssier, C., 2016. Guatemala paleoseismicity: from Late Classic Maya collapse to recent fault creep, *Sci. Rep.*, **6, 36976**, doi: 10.1038/srep36976.

Ellis, A. P., DeMets, C., Briole, P., Molina, E., Flores, O., Rivera, J., Lasserre, C., Lyon-Caen, H., & Lord, N., 2015. Geodetic slip solution for the M_w = 7.4 Champerico (Guatemala) earthquake of 2012 November 7 and its postseismic deformation, *Geophys. J. Int.*, **201**, 856–868, doi: 10.1093/gji/ggu484.

Harlow, G. E., Hemming, S. R., Lallemant, H. G. A., Sisson, V. B., & Sorensen, S. S., 2004. Two high-pressure-low-temperature serpentinite-matrix melange belots, Motagua fault zone, Guatemala: A record of Aptian and Maastrichtian collisions, *Geology*, **32**, 17–20.

Reinen, L. A., Weeks, J. D., & Tullis, T. E., 1991. The frictional behavior of serpentinite, *Geophys. Res. Lett.*, **18**, 1921–1924.

Ye, L., Lay, T., & Kanamori, H., 2013. Large earthquake rupture process variations on the Middle America megathrust, *Earth planet. Sci. Lett.*, **381**, 147—155.

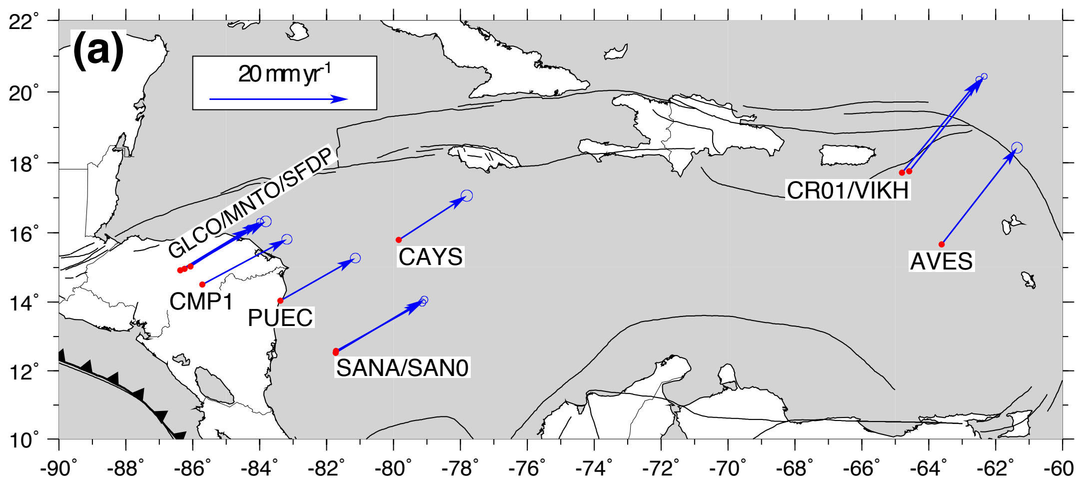

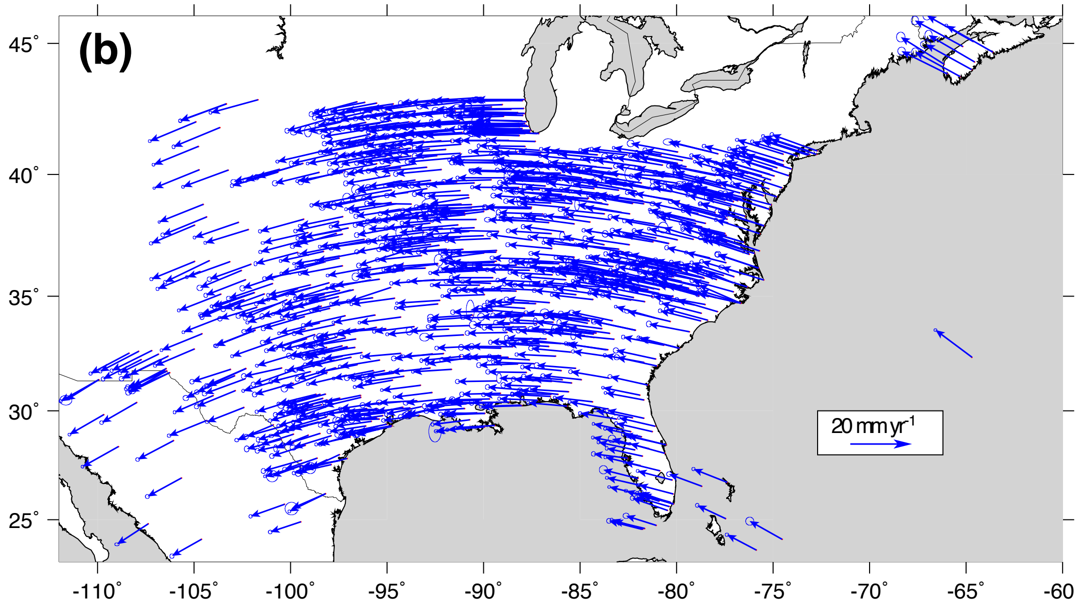

Supplementary Figure 1. (a) Locations, names, and velocities of the 11 GPS sites used in the analysis to estimate the Caribbean plate angular velocity relative to the International Terrestrial Reference Frame 2008 (Altamimi *et al*. 2011). All velocities are relative to ITRF08. The velocity ellipses show the 2-D, 1-sigma uncertainties. Site names are separated by slashes at locations with more than one closely-spaced GPS site. (b) Velocities relative to ITRF08 for all 989 GPS sites used herein to estimate the North America plate angular velocity relative to ITRF08.

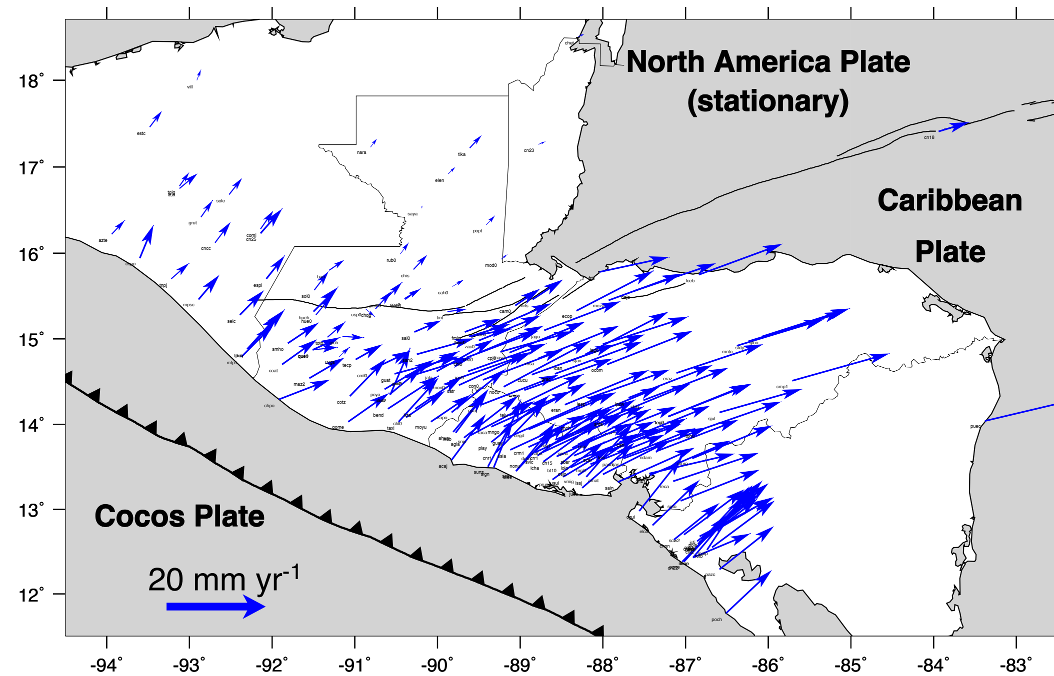

Supplementary Figure 2. New GPS site velocities relative to the North America Plate. Velocities are corrected for coseismic offsets and transient afterslip from the 2009 Swan Islands earthquake and the 2012 El Salvador and southern Guatemala (Champerico) earthquakes (Ellis *et al*. 2018). Error ellipses are omitted for clarity. GPS site names are printed adjacent to each site and can be viewed upon figure magnification.

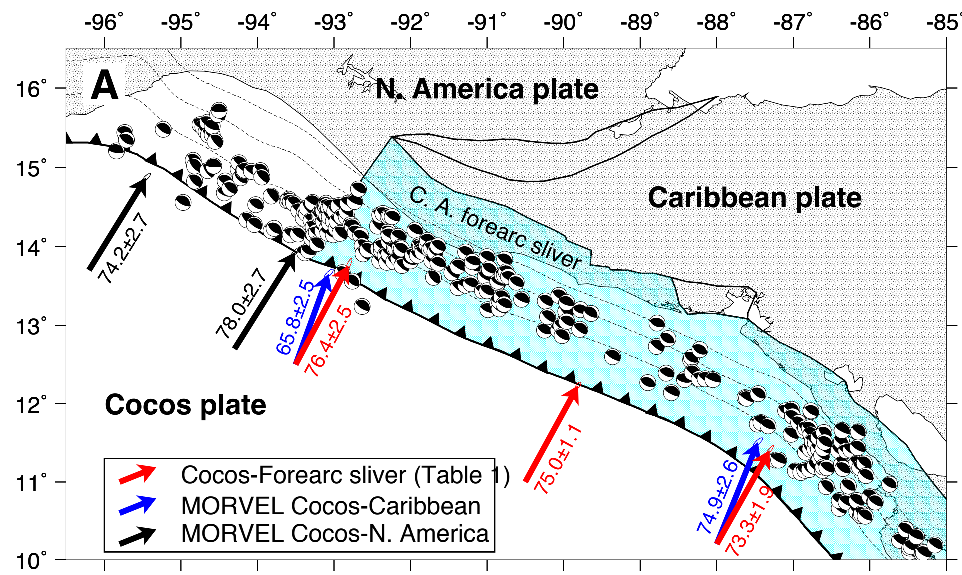

Supplementary Figure 3. 1976-2017 reverse-faulting earthquake focal mechanisms from the global centroid-moment tensor catalogue (Dziewonski *et al*. 1981; Ekstrom *et al*. 2012). The black, blue, and red arrows respectively show velocities that are predicted by the MORVEL Cocos-North America and Cocos-Caribbean angular velocities (DeMets *et al*. 2010) and our new angular velocity for the Cocos plate relative to the Central America forearc sliver (Table 1 in the main document). Velocities and 1-σ uncertainties are given in mm yr^{-1}.

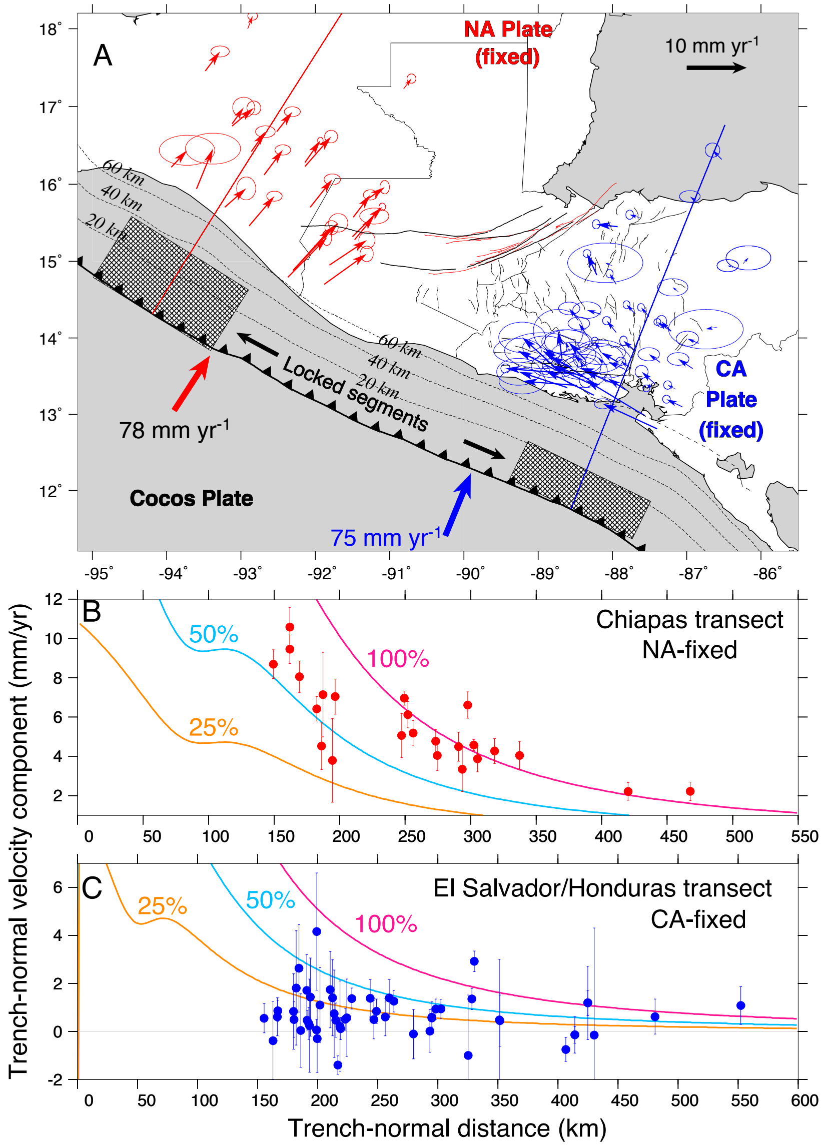

Supplementary Figure 4. (a) GPS site velocities relative to stationary North America (red) and Caribbean plates (blue). The dark gray areas identify the subduction interface patches that are locked at 25, 50, and 100 percent of the plate convergence rate for the elastic half-space models whose predictions are shown in (b) and (c). (b) Trench-normal (N32°E) velocity component versus distance to trench for GPS sites in the Chiapas/western Guatemala transect (red arrows in (a)). Elastic model predictions use a 78 mm yr^{-1} Cocos-North America convergence rate (Supplemental Fig. 3). (c) Trench-normal (N22°E) velocity component for GPS sites in the El Salvador/Honduras transect (blue arrows in (a)). Elastic model predictions use a 75 mm yr^{-1} Cocos-forearc sliver convergence rate (Supplemental Fig. 8). All uncertainties are 1-σ.

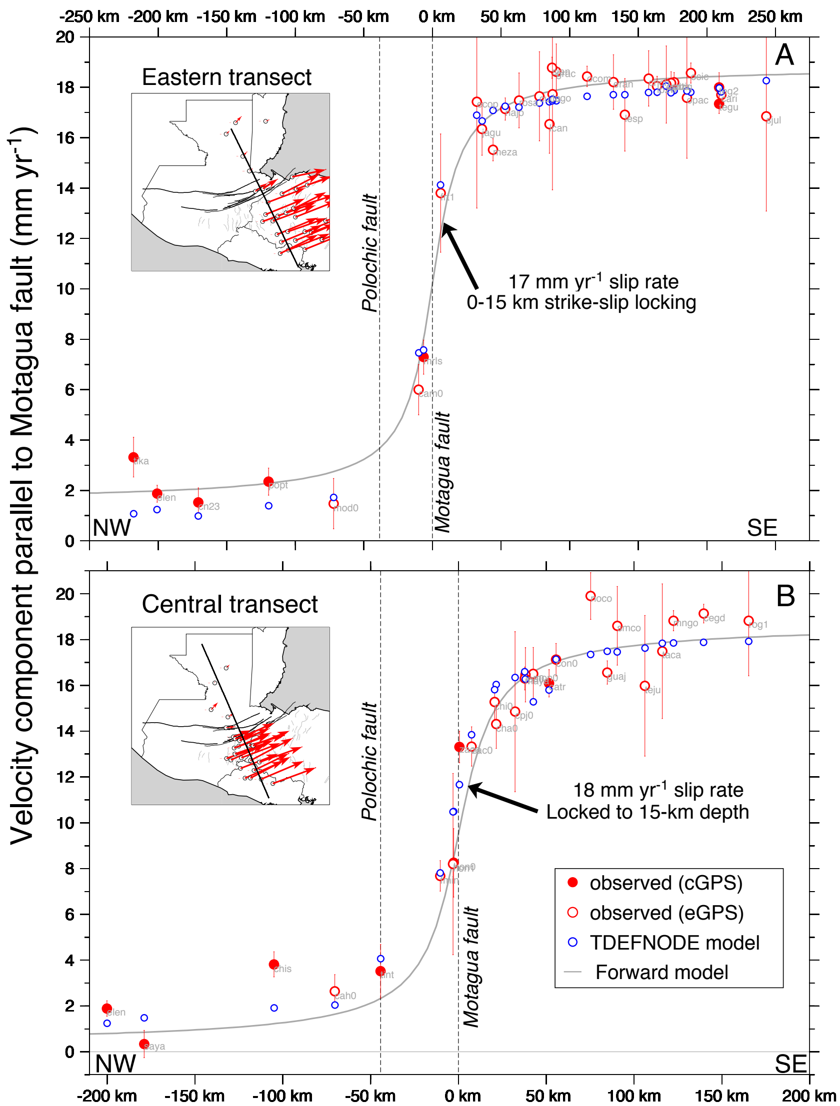

Supplementary Figure 5. Eastern (a) and central (b) Motagua-Polochic fault zone transects showing the observed (red) and modeled (blue) GPS site velocity components rotated onto respective fault-parallel azimuths of N62°E and N60.5°E. See legend in (b) for symbol interpretations. The inset maps identify the GPS sites in each transect and their velocities. Uncertainties are 1-σ. The TDEFNODE estimates are for our preferred model. The gray curves show predictions from an elastic half-space model that assumes 100 percent locking of the Motagua fault to a depth of 15 km. The North American plate is stationary. Abbreviations: cGPS, continuous GPS; eGPS, episodic GPS.

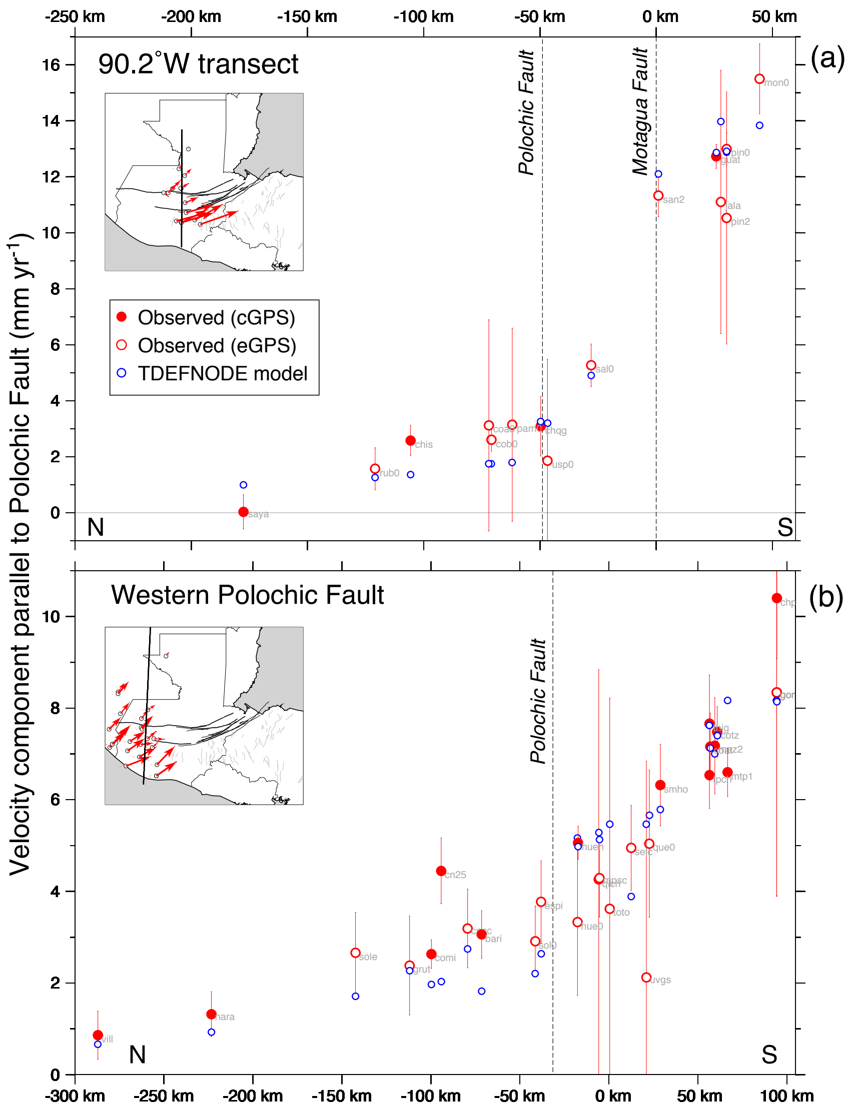

Supplementary Figure 6. Transects of the Motagua-Polochic fault zone at 90.2°W (A) and of the western Polochic Fault (B) with the observed (red) and modeled (blue) GPS site velocity components rotated onto N89°E (A) and S87°E (B), parallel to the Polochic Fault within each transect. The TDEFNODE model estimates are for our preferred model. The inset maps identify the GPS sites and their velocities for each transect, with velocities displayed relative to the North American plate. Uncertainties are 1-σ. Abbreviations: cGPS, continuous GPS; eGPS, episodic GPS.

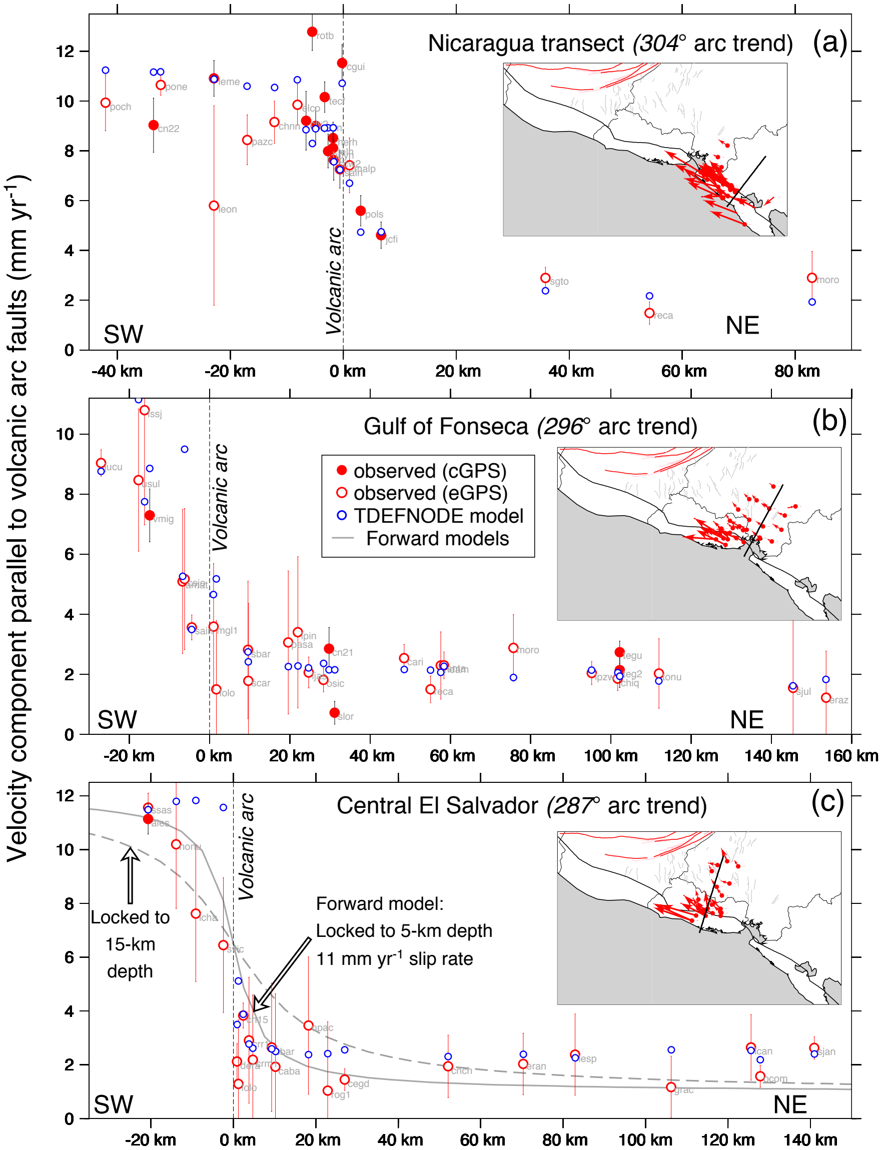

Supplementary Figure 7. Central America volcanic arc transects showing GPS site velocity components locally parallel to the volcanic arc. Inset maps show transect sites and velocities relative to the Caribbean plate. See legend for symbol interpretations. The TDEFNODE estimate is for our preferred model. Uncertainties are 1-σ. Gray curves show elastic half-space predictions for strike-slip faults fully locked to depths of 5 km and 15 km. Abbreviations: cGPS, continuous GPS; eGPS, episodic GPS.

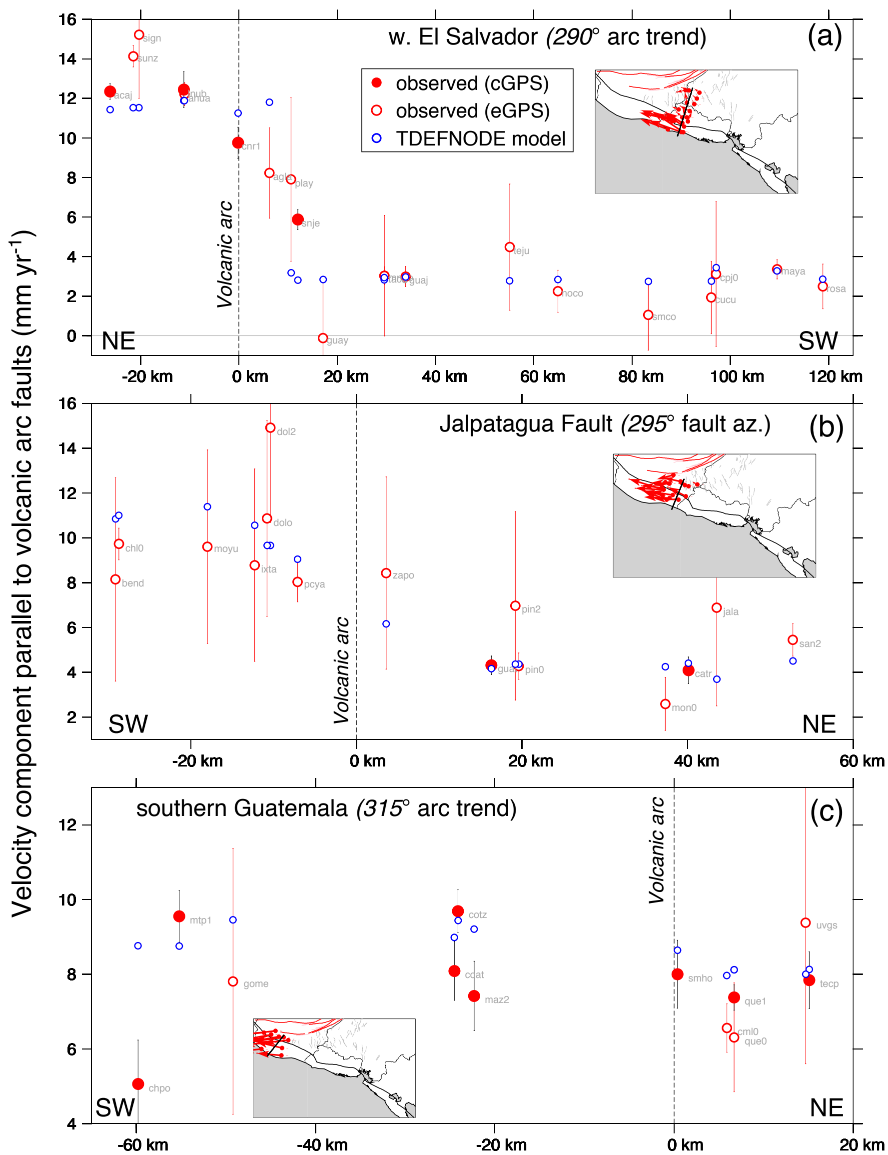

Supplementary Figure 8. Central America volcanic arc transects showing GPS site velocity components locally parallel to a fault or to the volcanic arc. Inset maps show transect sites and velocities relative to the Caribbean plate. See legend in (a) for symbol interpretations. The TDEFNODE estimate is for our preferred model. Uncertainties are 1-σ. Abbreviations: cGPS, continuous GPS; eGPS, episodic GPS.

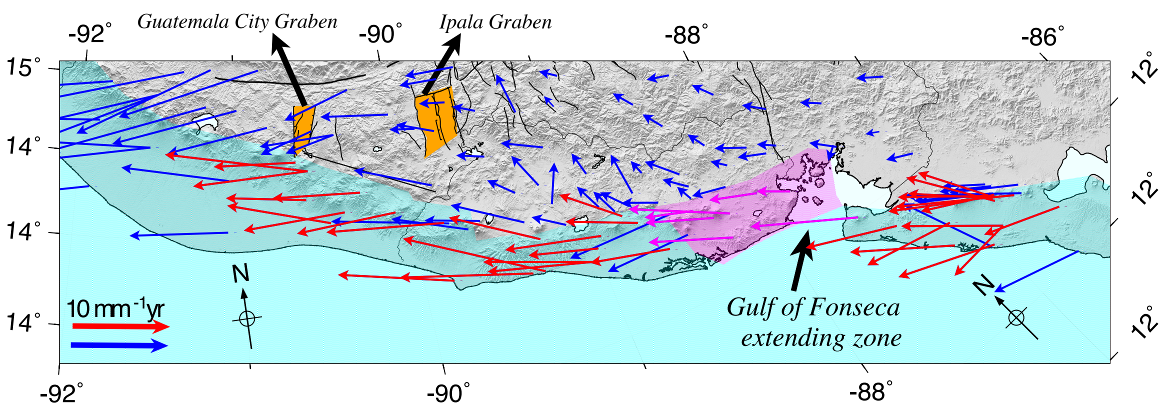

Supplementary Figure 9. Oblique Mercator projection of western Central America centered on 7.3°N, 91.4°W, the pole that best fits the directions measured for 33 GPS sites on the Central America forearc sliver (red velocity arrows) relative to the Caribbean plate. The limits of the Central America forearc sliver are depicted by the light-blue shaded region. The seven GPS sites whose directions are used to determine the pole of rotation for the Gulf of Fonseca block are colored magenta.

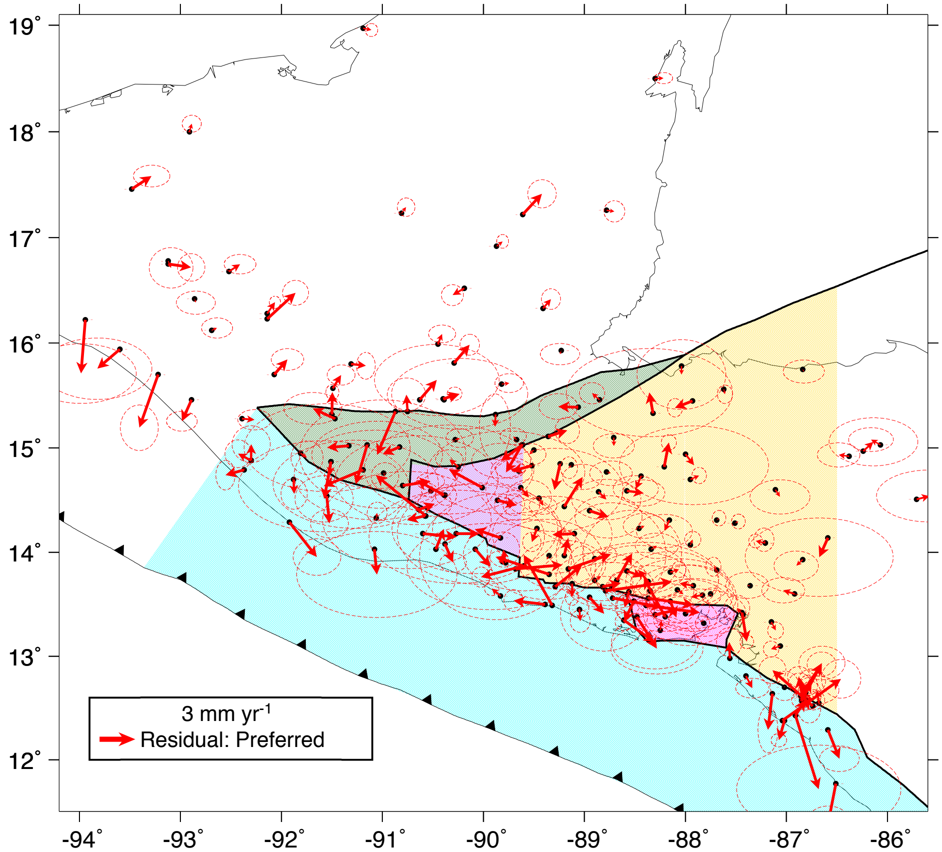

Supplementary Figure 10. Summary map of residual GPS site velocities for the preferred TDEFNODE inversion (see text). Residual velocities are the modeled velocities subtracted from the observed velocities. Shading identifies the blocks used for our preferred model. Uncertainty ellipses are 2-D, 1-σ.

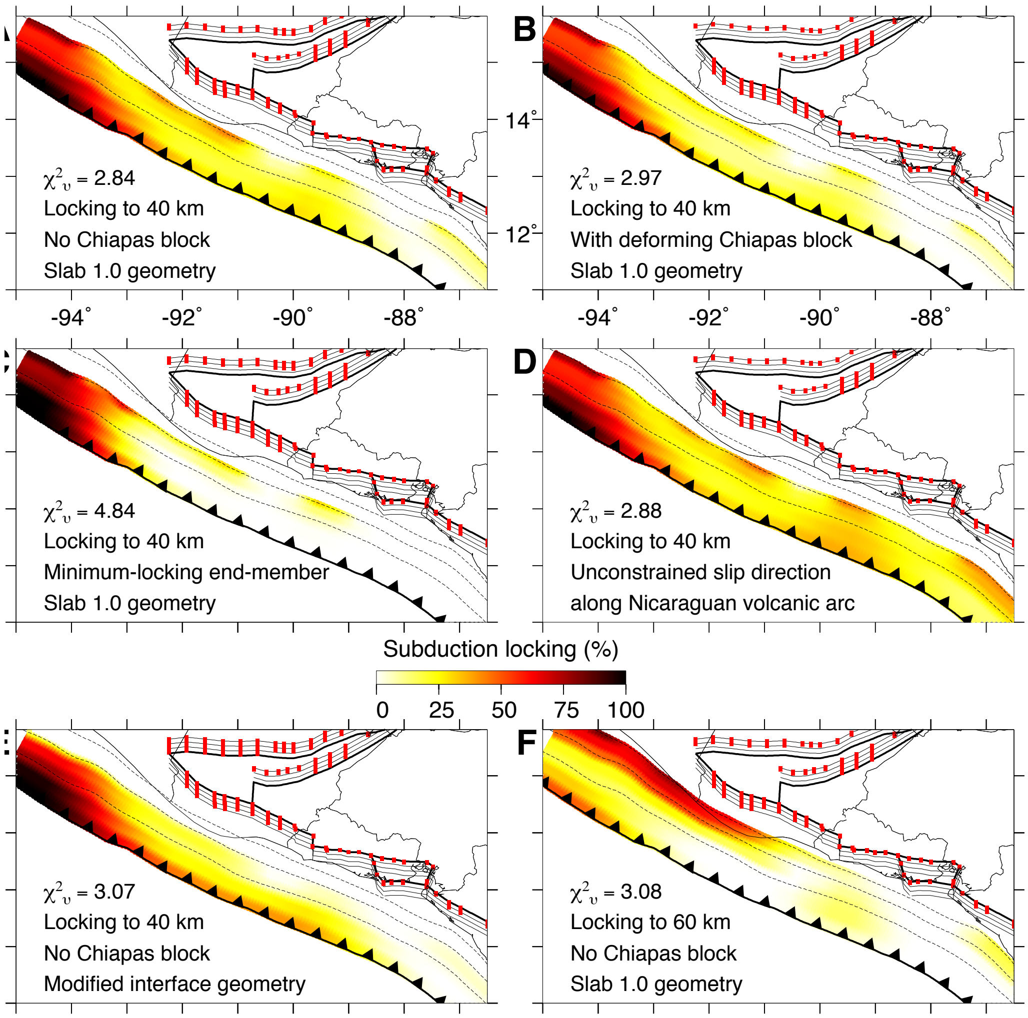

Supplementary Figure 11. Influence of modeling assumptions on the estimated interseismic locking and model fit, as given by reduced chi-square ($\chi^2{}_\nu$). (a) Preferred model results, which restrict subduction locking to depths above 40 km, exclude the Chiapas block, and use the Slab 1.0 interface geometry of Hayes *et al*. (2012). (b) Same as (a), but for a model with a separate, deforming Chiapas block. (c) Weak-locking end-member model described in text. (d) Same as (a), but for a model without any constraints on slip direction along the volcanic arc in Nicaragua (see text). (e) Same as (a), but for a model with a more curved subduction interface (see text). (f) Same as (a), but for model with subduction locking down to 60 km.

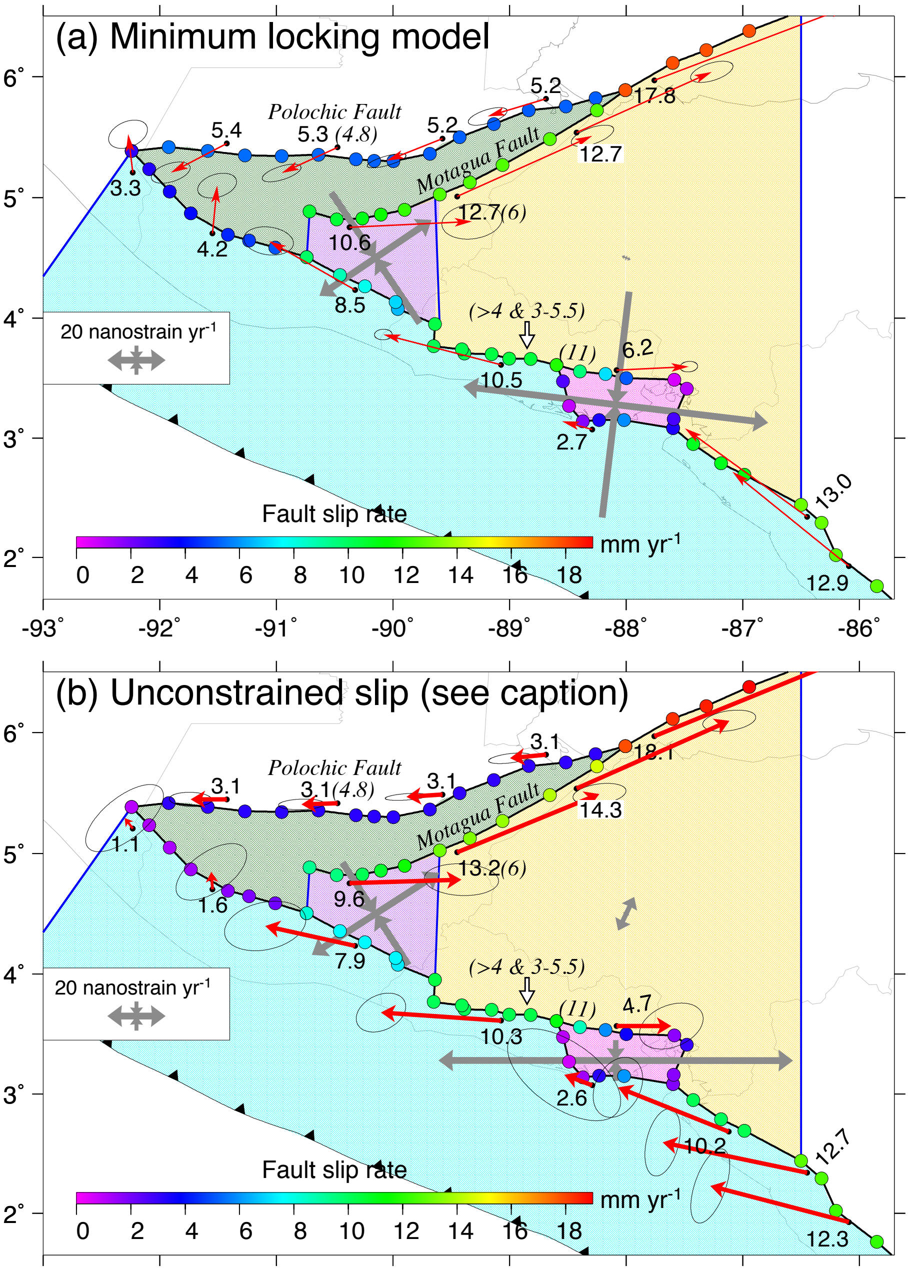

Supplementary Figure 12. Estimates of fault slip rate and block strain rates for alternative TDEFNODE models C and D from Supplemental Fig. 10 (shown in (a) and (b, respectively). The model in (a) is the minimum-locking end-member model described in the text. The model in (b) excludes any constraints on the relative slip direction along the Nicaraguan volcanic arc. The slip rates estimated at the strike-slip fault nodes are color coded according to the scale on the map. The red arrows and their adjacent numbers show the velocities estimated for the plate or block on which each arrow originates relative to the plate or block across the adjacent strike-slip fault. Slip rates have units of mm yr^{-1}. If available, published geologic fault slip rates are given parenthetically. The gray double-headed arrows show the estimated strain-rate axes, with outward-pointing arrows indicating extensional strain rates.

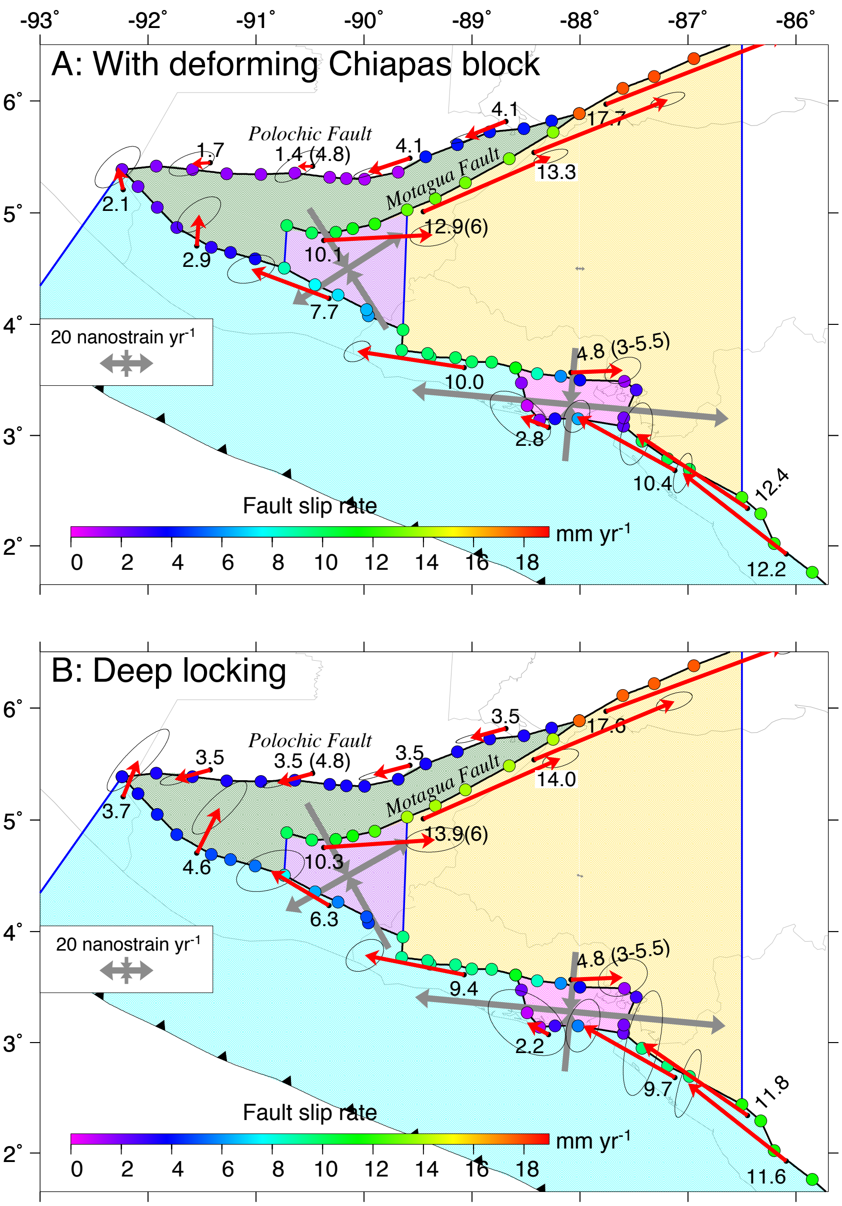

Supplementary Figure 13. Estimates of fault slip rate and block strain rates for alternative TDEFNODE models B and F from Supplemental Fig. 10 (shown in (a) and (b), respectively). The model in (a) includes a deforming, Chiapas block in the block configuration. The model in (b) permits locking of the subduction interface to extend downward to 60 km, 20 km deeper than our preferred model. The slip rates estimated at the strike-slip fault nodes are color coded according to the scale on the map. The red arrows and their adjacent numbers show the velocities estimated for the plate or block on which each arrow originates relative to the plate or block across the adjacent strike-slip fault. Slip rates have units of mm yr^{-1}. If available, published geologic fault slip rates are given parenthetically. The gray double-headed arrows show the estimated strain-rate axes, with outward-pointing arrows indicating extensional strain rates.